Detailed Study of Rolling Bearing Element Faults in Rotating Electrical Machines using MVSA Technique

Noureddine Bessous[1*], Salim Sbaa[2], Radouane Bousseksou[1], Abdelkrim Allag[1]
1- Department of Electrical Engineering, University of El-Oued, Algeria.
Email: nbessous@yahoo.fr (Corresponding author)
2- Department of Electrical Engineering, University of Mohamed Khider,Biskra, Algeria.
Email: s_sbaa@yahoo.fr

Received: October 2018 Revised: December 2018 Accepted: April 2019

ABSTRACT:
This paper presents the mechanical fault detection in Squirrel Cage Induction Motors (SCIMs). In this study, we diagnosed the Rolling Bearing Element (RBE) faults in SCIM. Rolling bearing element faults is a major problem among different faults, which cause catastrophic damage to rotating machinery. thus, early detection of the RBE faults in SCIMs is a very important step. Among the key words of the mechanical vibrations for rotating electrical machines is the vibration analysis. This technique is generally called Motor Vibration Signature Analysis (MVSA) which is based on the vibration image. The vibration signal analysis is a one of the most important methods in the fault detection field. MVSA is generally based on Fast Fourier Transform (FFT) of the vibration signal. This research work has utilized the MVSA-FFT in detail, in order to detect the RBE faults. In addition, this study shows a new overlap between the characteristic frequencies of the RBE faults. In order to make an accurate analysis; it is important to know this overlap in advance. This new overlap has the advantage of expressing it by specific formulas which allows us to verify the additional harmonics carefully. The acquisition data is performed experimentally in order to ensure a wise decision.

KEYWORDS: Induction Motor, Fault Detection, Motor Vibration Signature Analysis, Outer Race Fault, Inner Race Fault, Fast Fourier Transform, Vibration Signal Spectrum.

1. INTRODUCTION

Because of its advantages, the squirrel cage induction motors are used more than 90% in the industrial or domestic sector when comparing it with other motor types. But like any other machine, SCIMs can affect multiple faults under different causes. According to the constituent elements of the SCIM, we can notice the percentage faults in Fig. 1 [1]:

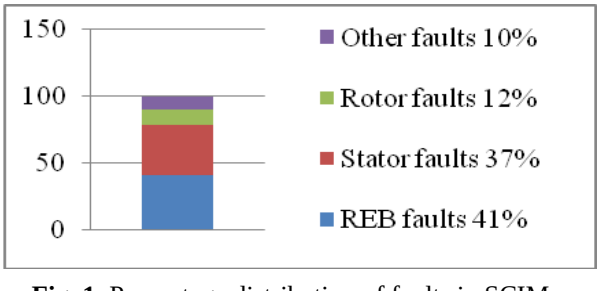

Fig. 1. Percentage distribution of faults in SCIMs.

Rotating electrical machine monitoring is a very important step in order to: avoid damage, increase the system life, etc. Among the faults which can affect rotating machines, we quote: the imbalance voltage, the rotor or stator eccentricity, the broken rotor bars, the short circuit in the stator and the RBE faults [2-7].

In order to detect different faults, we found several techniques which are used in the diagnostic field [8-10]. A great competition between the researchers is accelerating to lead to a simple, efficient and precise technique in the field of diagnosis of rotating machines.

Many works are concerned on the development of an analytical model which leads a good simulation [11], [12].

One of the simple techniques that occupy currently a large part of the industry is the vibration analysis which is based on the vibration image in order to analyse their content. This analysis technique is often called: Motor Vibration Signature Analysis (MVSA) [13, 14]. In addition, these vibrations have several influences on the electromagnetic phenomena in the SCIMs. For this purpose, the cancellation of harmonics under a control system is the goal of many works [15].

In fact, the goal of several vibration signal processing methods is to fault detection in rotating electrical machines in an early stage.

A detailed study of the bearing failure by the spectral analysis of the vibration signal has been made carefully. The Fast Fourier Transform (FFT) of the vibration signal allows us to extract the characteristic frequencies of the RBE faults. In addition, we have indicated new harmonic formulas that are responsible for the overlap between some faults. The knowledge of these formulas is a crucial step to make a good diagnosis.

We did an experimental part which ensures the acquisition of the vibration signal. In this regard, the basic principles for the RBE faults detection using the MVSA-FFT analysis of the vibration signal are explained in the following sections.

2. TECHNICAL WORK PREPARATION

In this study, we used SCIM which has a characteristic as follow: 3kW, p=2 (number of pole pairs), f_s=50Hz and 28 bars. Fig. 2 shows the induction motor with some equipment in order to take the measurements.

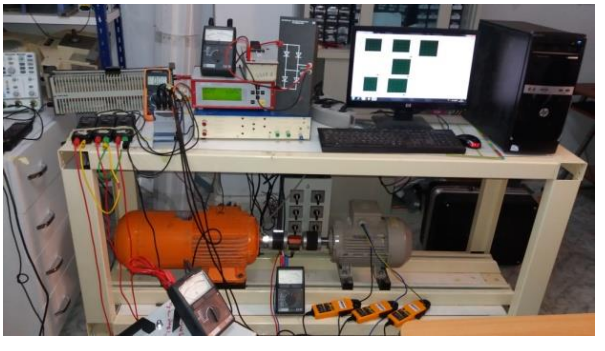

Fig. 2. Experiment setup dedicated to RBE faults.

We realized two RBE fault types: the Outer Raceway Fault (ORF) and the inner raceway fault (IRF). Photos in Fig. 3 illustrates the bearing element faults. The bearing elements type of our induction motor (3kW) is single-row ball and angular contact. It belongs to the 6206 series which has 9 balls.

Fig. 3. Photos of ORF and IRF.

3. TECHNICAL WORK PREPARATION

So far, there has been no approach in the analysis and final elimination of vibrations and/or noises. Vibration is considered one of the important goals to achieve monitoring.

Recently, vibration analyses of rotating electrical machines have been used by industrialists for diagnosing faults. The identification of the problem makes it possible to set up curative actions such as a setting or the replacement of a defective part before the breakdown of the machine. The MVSA of the electric motor is one of the means which is used to monitor the health of rotating machinery in operation.

Our goal is to study the RBE fault detection based on the MVSA technique; that is, by analyzing the vibration images induced by these faults. The knowledge of these vibration images and the kinematics of the machine will allow us to formulate a judicious decision.

Generally, the RBE consists of four elements as shown in Fig. 4:

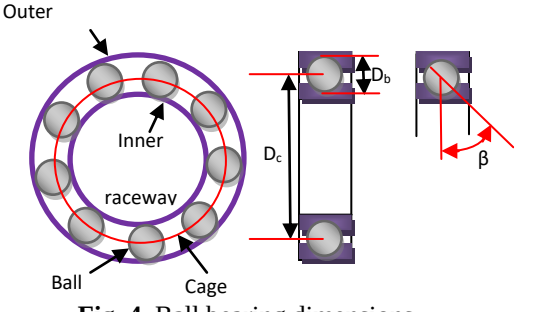

Fig. 4. Ball bearing dimensions.

In this study, we are interested to detect two fault types of the RBE:

- The Outer Raceway Fault (ORF);
- The Inner Raceway Fault (IRF).

We have taken into consideration the operating conditions of the induction motor: at no-load operation and at load operation.

Note: In this study, all which is simulated in blue designates the healthy state and all which is in red indicates the faulty state.

The method is employed to test the efficiency of the vibration analysis. The bearing element fault detection lies on the experimental comparison between the vibration signal spectrum in healthy and faulty state. The characteristic frequencies ($f_{ch\text{-}vib}$) in the spectra of vibration signal are verified by the following formula:

- Outer raceway:

$$f_{ch-vib-OR} = f_{OR} = \frac{N_b}{2} f_r \left(1 - \frac{D_b}{D_c} \cos\beta\right) \quad (1)$$

- Inner raceway:

$$f_{ch-vib-IR} = f_{IR} = \frac{N_b}{2} f_r \left(1 + \frac{D_b}{D_c} \cos\beta\right) \quad (2)$$

- Ball:

$$f_{ch-vib-Ball} = f_B = \frac{D_c}{D_b} f_r \left(1 - \frac{D_b^2}{D_c^2} \cos^2 \beta\right) \quad (3)$$

- Cage:

$$f_{ch-vib-Cage} = f_C = \frac{f_r}{2}\left(1 - \frac{D_b}{D_m}\cos(\beta)\right) \quad (4)$$

The bearing element geometry is mentioned in Fig. 4.

It has been statistically shown in [8] that the characteristic frequencies can be approximated for most bearing elements with ball numbers between 6 and 12 by:

$$f_{OR} = 0.4 N_b \times k \times f_r \quad (5)$$

$$f_{IR} = 0.6 N_b \times k \times f_r \quad (6)$$

where,

$k = 1, 2, 3, \ldots$, f_s is the supply frequency, f_r is the mechanical rotor frequency and N_b is the number of balls equal 9.

3.1. Outer Raceway Detection

The vibration signal of a shock due to an ORF is shown in Fig. 5. The time signal for a no-load operation (s=0.004≈0) will be analyzed by the fast Fourier transform. It allows us to discover the new harmonics due to the ORF. Fig. 6 shows the spectrum of the two states of the SCIM: healthy in blue and faulty in red. To clarify the fault indices, we present a zoom for different frequency ranges. Fig. 7 shows the frequencies due to the ORF with its amplitudes.

The different frequency bands help us to use the signal correctly to reach a final decision on the SCIM situation. The part of the lower frequencies (Fig. 7-c-d-e) shows the existence of the characteristic frequencies in accordance with the formula (5). However, it is essential to indicate some formulas of overlap between other faults in RBE. According to the frequency formulas which characterize the RBE faults, and for a good detection; it is necessary to distinguish the frequencies which have the same value. From this reason, we propose these formulas which show the points of intersection between the characteristic frequencies to be detected for: ORF, IRF and cage faults.

$$\begin{cases} 3k \times f_{OR} = 2k \times f_{IR} \\ k \times f_{OR} = 9k \times f_C \\ 2k \times f_{OR} = 27k \times f_C \end{cases} \quad (7)$$

with, k=1, 2, 3,…etc.

These formulas lead us to avoid any confusion in the spectrum to be analyzed. Either this following illustrative example:

We will take this case which deals with the ORF and IRF. If the slip is equal to 0.004 (f_r=24.9 Hz) for a no-load motor operation, we thus obtain: f_{OR}=0.4×(9)×f_r and f_{IR}=0.6×(9)×f_r.

Therefore, the value of 3×f_{OR}=268.92 Hz which is equal to the value of 2×f_{IR}=268.92 Hz. The knowledge of these intersections leads to a more precise detection.

The characteristic frequencies of the ORF have successively appeared clearly with remarkable amplitude. The frequencies which characterize this fault are: 1×f_{OR}=89.64 Hz, 2×f_{OR}=179.28 Hz, 3×f_{OR}=268.92 Hz, 4×f_{OR}=358.56 Hz, 5×f_{OR}=448.2 Hz, 6×f_{OR}=537.84 Hz, etc.

We have also noticed several harmonic peaks (sideband frequencies) which spaced around the characteristic frequencies by the following formula [16]:

$$f_{SBF-OR} = k \times f_{OR} \pm k' \times f_r \quad (8)$$

With, k and k' are integers.

These values of the sideband frequencies (f_{SBF-OR}) will be changed systematically for a motor that operates under load.

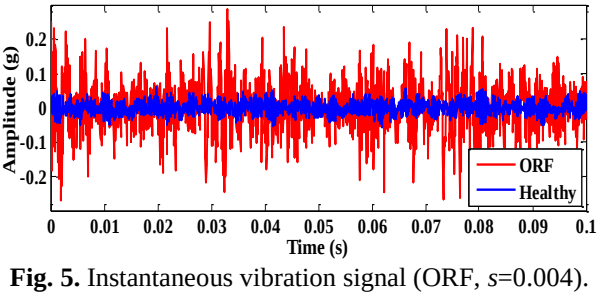

Fig. 5. Instantaneous vibration signal (ORF, s=0.004).

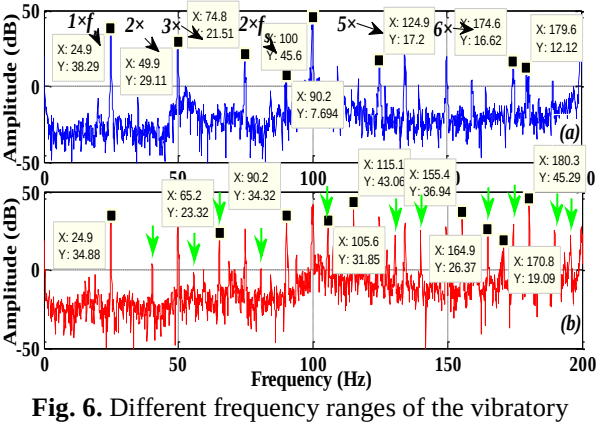

Fig. 6. Different frequency ranges of the vibratory signal spectrum (ORF, s=0.004).

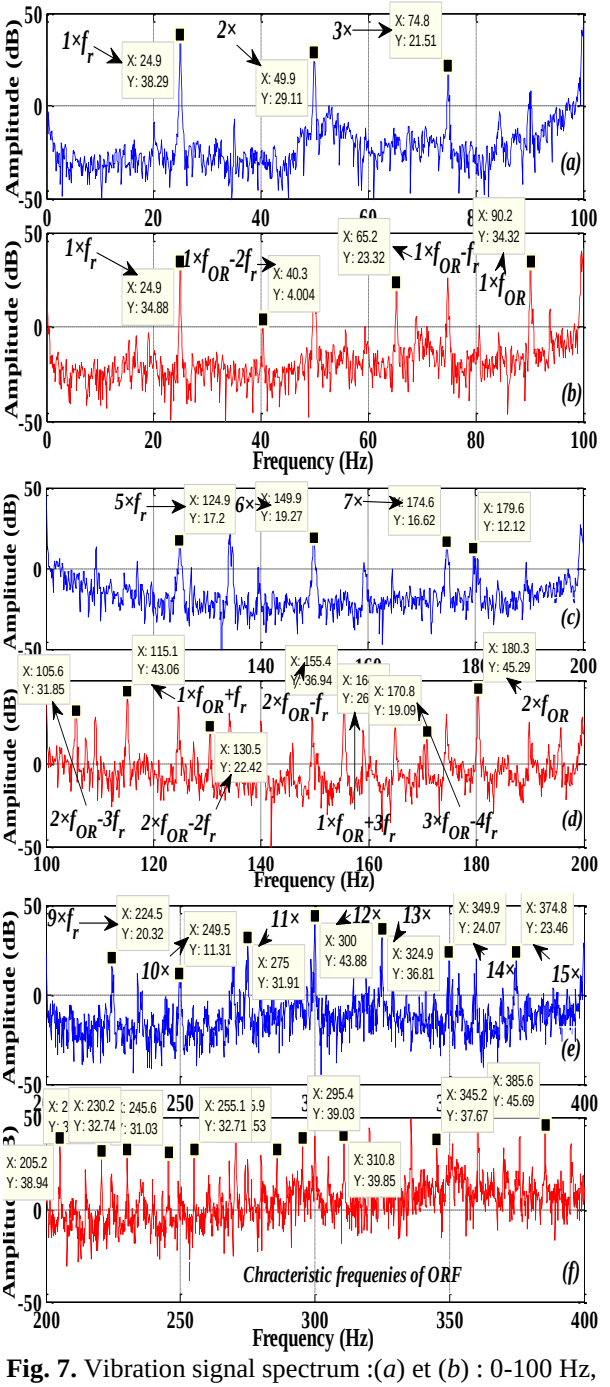

Fig. 7. Vibration signal spectrum :(*a*) et (*b*) : 0-100 Hz, (*c*) et (*d*) : 100-200 Hz, (*e*) et (*f*) : 200-400 Hz (ORF, *s*=0.004).

Vibration signal spectrum is very rich in information concerning the SCIM state under ORF. The frequencies linked with $k\times f_{OR}$ are well determined. The table below summarizes some characteristic frequencies with its amplitudes.

Table 1. Recapitulation of some theoretical and practical harmonics in the vibration signal spectrum (ORF, *s*=0.004).

Formulae of f_{OR}	Theoretical Values [Hz] (s=0.004)	Practical Values [Hz] (s=0.004)	Amplitude [dB]	
			Healthy	ORF
$1\times f_{OR}$	*89.64*	*90.2*	*7.69*	***34.32***
$2\times f_{OR}$	*179.28*	*180.3*	*12.12*	***45.29***
$1\times f_{OR}-2f_r$	*39.84*	*40.3*	/	***4.004***
$1\times f_{OR}-f_r$	*64.74*	*65.2*	/	***23.32***
$2\times f_{OR}-3f_r$	*104.58*	*105.6*	/	***31.85***
$1\times f_{OR}+f_r$	*114.54*	*115.1*	/	***43.04***
$1\times f_{OR}+3f_r$	*164.34*	*164.9*	/	***26.3***

The variation of the load causes a variation in the speed of rotation, so in sliding value. A load torque of 75% is applied to the SCIM; it makes the slip at the value *s*=0.032. In this case, the characteristic frequency values will be moved. The temporal signal of the vibration signal is shown in Fig. 8. The spectrum of the vibration signal of the Fig. 9 presents the frequencies: 87.12Hz, 174.24Hz, 261.36Hz, 348.48Hz, 435.6Hz, etc. They are verified the formula of ORF frequencies. The other frequency ranges confirm the accuracy of the theoretical and the practical results.

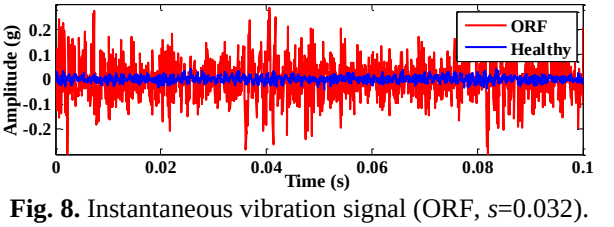

Fig. 8. Instantaneous vibration signal (ORF, *s*=0.032).

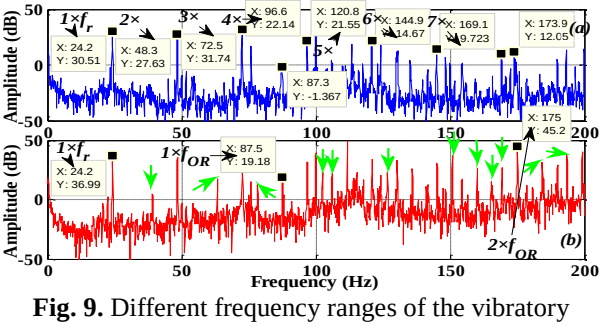

Fig. 9. Different frequency ranges of the vibratory signal spectrum (ORF, *s*=0.032).

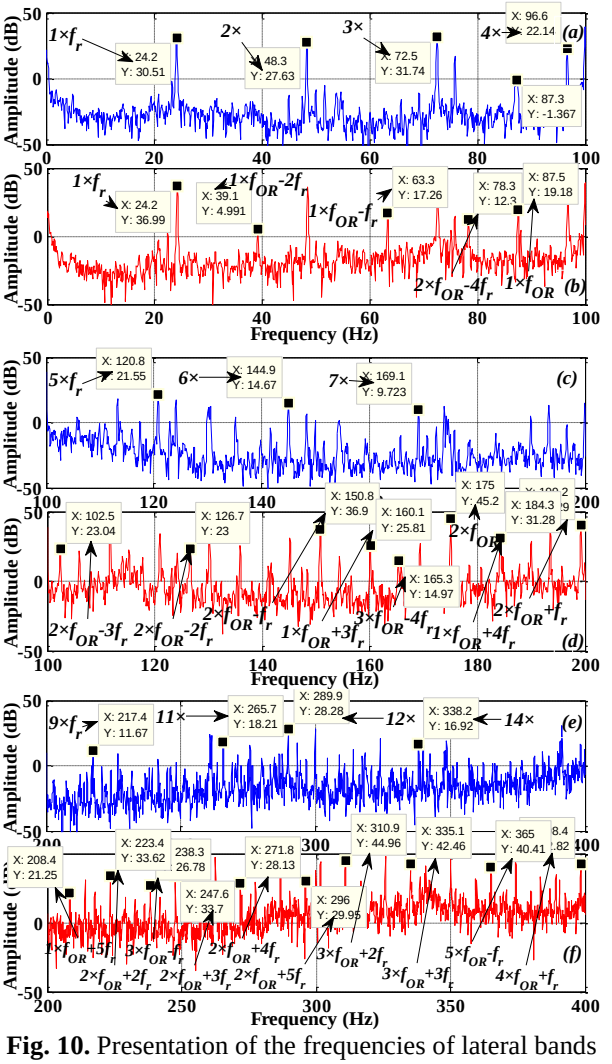

Fig. 10. Presentation of the frequencies of lateral bands around $k\times f_{OR}$ in the spectrum of the vibratory signal (OR, s=0.032).

All the frequencies shown in the Fig. 10-f are connected with the formula (5). Based on this analysis, we found the SBFs values around the characteristic frequencies of the ORF. In addition, the spectrum of the vibration signal is rich in harmonics for advanced ranges of frequency (higher frequencies). Fig. 10 shows these two interesting points. Fig. 11 illustrates the appearance of significant frequencies at the bearing fault when an amplitude margin of more than 0 dB is allowed

Table 2 summarizes a set of harmonics characterizing the ORF.

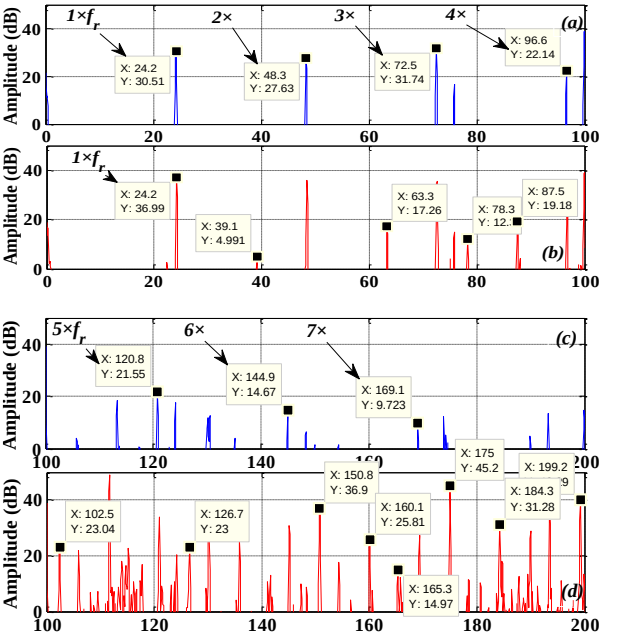

Fig. 11. Zoom presentation of the sideband frequencies around $k\times f_{OR}$ in the spectrum of the vibratory signal (OR, s=0.032).

Table 2. Recapitulation of some theoretical and practical harmonics in the vibration signal spectrum (ORF, s=0.032).

Formulae of f_{OR}	**Theoretical Values [Hz] (s=0.032)**	**Practical Values [Hz] (s=0.032)**	**Amplitude [dB]**	
			Healthy	**ORF**
$1\times f_{OR}$	*87.12*	*87.5*	*-1.36*	***19.18***
$2\times f_{OR}$	*174.24*	*175*	*12.05*	***45.2***
$1\times f_{OR}-2f_r$	*38.72*	*39.1*	*/*	***4.99***
$1\times f_{OR}-f_r$	*62.92*	*63.3*	*/*	***17.26***
$2\times f_{OR}-4f_r$	*77.44*	*78.3*	*/*	***12.3***
$2\times f_{OR}-3f_r$	*101.64*	*102.5*	*/*	***23.04***
$3\times f_{OR}+3f_r$	*333.96*	*335.1*	*/*	***42.46***

According to this part which is based on the MVSA technique, we can say that the important values of the characteristic frequencies are visible. Therefore, the analysis of the vibration signal spectrum allowed us to detect the outer race fault easily.

3.2. Inner Raceway Detection

To determine the nature of the IRF, we follow the same steps of the spectral analysis of a vibration signal. Fig. 12 presents the instantaneous values of the vibration signal for two operating regimes. The verification of the characteristic frequencies of the IRF is presented in Fig. 12 for a no-load operation (s=0.004, f_r =24.9 Hz).

In Fig. 13, the additional harmonics are very clear. They are logical with the formula (I.18). In addition, sideband frequencies (SBFs) around the characteristic frequencies are in correspondence with the following formula [16]:

$$f_{SBF-IR} = k \times f_{IR} \pm k' \times f_r \quad (9)$$

With, k and k' are integers.

The observation of the spectrum, for different frequency ranges, shows the effectiveness of the MVSA technique. The characteristic frequencies of IRF were calculated as a function of the rotational speed (f_r) and the characteristics of the bearing (N_b=9).

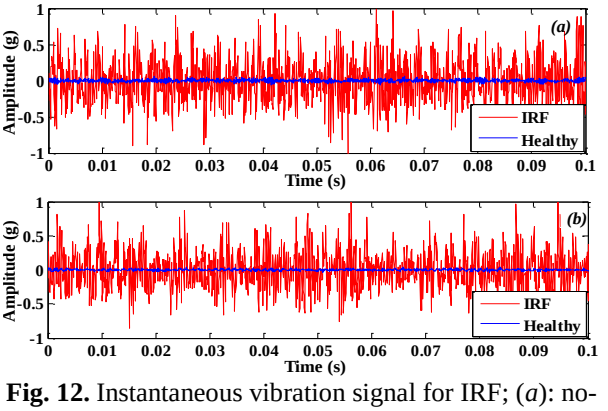

Fig. 12. Instantaneous vibration signal for IRF; (*a*): no-load, (*b*): 75% of the load.

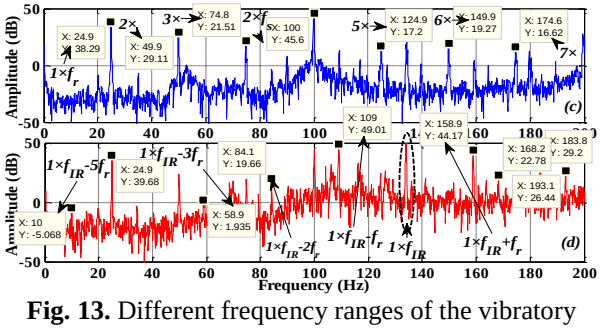

Fig. 13. Different frequency ranges of the vibratory signal spectrum (IRF, s=0.004).

We zoom in around different frequency ranges in order to visualize the additional harmonics due to the IRF.

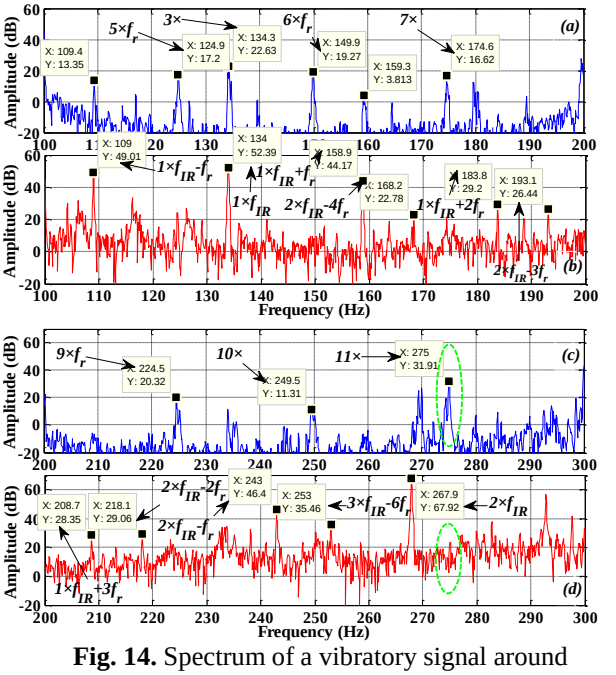

Fig. 14. Spectrum of a vibratory signal around different frequency ranges (IRF, s=0.004).

A presentation of some characteristic harmonics with their amplitude values is summarized in the following table:

Table 3. Recapitulation of some theoretical and practical harmonics in the vibration signal spectrum (IRF, s=0.004).

Formulae of f_{IR}	**Theoretical Values [Hz] (s=0.004)**	**Practical Values [Hz] (s=0.004)**	**Amplitude [dB]**	
			Healthy	**IRF**
$1\times f_{IR}$	*134.46*	*134*	*22.63*	***52.39***
$2\times f_{IR}$	*268.92*	*267.9*	*2.08*	***67.92***
$1\times f_{IR}-3f_r$	*59.76*	*58.9*	*/*	***1.93***
$1\times f_{IR}-2f_r$	*84.66*	*84.1*	*-3.07*	***19.66***
$1\times f_{IR}+f_r$	*159.36*	*158.9*	*3.81*	***44.17***
$2\times f_{IR}-3f_r$	*194.22*	*193.1*	*/*	***26.44***
$3\times f_{IR}-6f_r$	*253.98*	*253*	*/*	***35.46***

We now present the vibration signal spectrum under 75% of the load (s=0.032). The vibration signal is the identity of the induction motor which is linked at each moment to the operating conditions. We can go to spectral analysis to confirm the signatures of the IRF.

Fig. 15 shows the FFT of the vibration signal for different frequency ranges. We notice that the harmonic values characterizing the IRF are appearing clearly. It shows the effectiveness of the MVSA-FFT technique.

SBFs around kf_{IR} exist along the spectrum by $kf_{IR}\pm k'f_r$; with f_r=24.2Hz (and s=0.032). Moreover, these characteristic frequencies appear clearly, even for more advanced frequency ranges. Among them, we obtain: 498.52 Hz, 546.92 Hz, 759.88 Hz, 808.28 Hz, 905.03 Hz, etc.

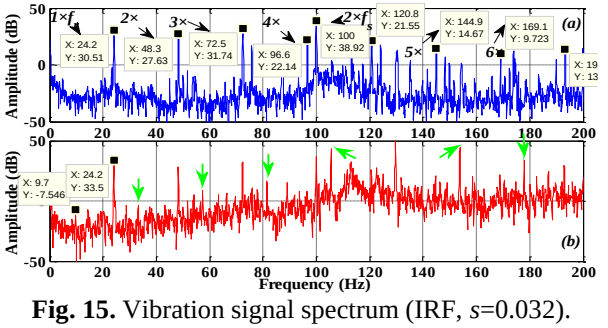

Fig. 15. Vibration signal spectrum (IRF, *s*=0.032).

The results obtained ensure the accuracy of the characteristic frequency values in the vibration signal spectrum for the IRF. The additional frequencies of the IRF are numerous throughout the spectrum.

Table 4 presents some theoretical and practical harmonic values regarding the IRF.

RBE faults are dominant in the industry of a significant percentage. Our analysis which based on MVSA-FFT confirms the effectiveness of fault detection in the rotating machines.

Table 4. Recapitulation of some theoretical and practical harmonics in the vibration signal spectrum (IRF, *s*=0.032).

Formulae of f_{IR}	**Theoretical Values [Hz] (s=0.032)**	**Practical Values [Hz] (s=0.032)**	**Amplitude [dB]**	
			Healthy	***IRF***
$1\times f_{IR}$	*130.68*	*129.7*	*12.78*	***54.03***
$2\times f_{IR}$	*261.36*	*267.9*	*2.08*	***67.92***
$1\times f_{IR}-3f_r$	*58.08*	*57.3*	*/*	***8.45***
$1\times f_{IR}-2f_r$	*82.28*	*81.4*	*/*	***16.74***
$1\times f_{IR}-f_r$	*106.48*	*105.6*	*4.07*	***42.98***
$1\times f_{IR}+f_r$	*154.88*	*153.8*	*1.41*	***44.54***
$1\times f_{IR}+2f_r$	*179.88*	*177.9*	*/*	***33.67***

We have studied the case of the ball bearings under different operating conditions (at no-load and at the load IM). The ORF gave good indices in the spectrum of vibration signals. The same positive results were obtained for the IRF. This explains the effectiveness of the MVSA-FFT method in the diagnosis field.

4. CONCLUSION

The observation of vibration signal is widely used in industry in order to detect many faults. The motor vibration signature analysis which is presented in this study has good indicators on the mechanical fault in induction motor type. For this reason, the MVSA is preferred until now for the fault detection in rotating machines.

Our work verified the additional harmonics carefully. In addition, we have indicated to a new overlap formulas. These formulas are mandatory to know them by the specialists who use the MVSA technique.

Because of the disadvantages of FFT analysis; many important information in the non-stationary or semi-stationary signal can be flexibly exploited by other signal processing technique.

5. ACKNOWLEDGMENT

This research was partially supported by the Electrical Engineering Laboratory of Biskra (LGEB), University of Mohamed Khider Biskra, BP 145 RP, 07000 Biskra, Algeria. We thank our colleagues from LGEB who provided insight and expertise that greatly assisted the research, although they may not agree with all of the interpretations/conclusions of this paper.

REFERENCES

[1] W.T. Thomson, **"A Review Of On-Line Condition Monitoring Techniques For Three-Phase Squirrel-Cage Induction Motors –Past, Present and Future,"** in *Proc. IEEE Int. Symp. SDEMPED* 1, pp. 3–18, 1999.

[2] A. Ebadi, M. Mirzaie, and S. A. Gholamian, **"Investigation of the Effects Of Unbalanced Voltages On The Performance Of A Three-Phase Squirrel Cage Induction Motor Using Finite Element Method,"** *Majlesi Journal of Electrical Engineering*, 7(2), pp. 76-82. 2013.

[3] N. Bessous, S. E. Zouzou, S. Sbaa, and W. Bentrah, **"A Comparative Study Between the MCSA, Dwt and The Vibration Analysis Methods to Diagnose the Dynamic Eccentricity Fault in Induction Motors,"** *in Systems and Control Conference (ICSC), IEEE*, pp. 414-421, 2017.

[4] A. M. Júnior, V. V. Silva, L. M. Bacarini, and L. F. Mendes, **"The Design of Multiple Linear Regression Models Using A Genetic Algorithm To Diagnose Initial Short-Circuit Faults in 3-Phase Induction Motors,"** *Applied Soft Computing*, pp. 50-58, 2018.

[5] G. Singh and V. N. A. Naikan , **"Detection of Half Broken Rotor Bar Fault in VFD Driven Induction**

Motor Drive Using Motor Square Current Music Analysis," *Mechanical Systems and Signal Processing*, pp. 333-348, 2018.

[6] N. G. Lo, A. Soualhi, M. Frini, H. Razik, **"Gear and Bearings Fault Detection Using Motor Current Signature Analysis,"** *in Industrial Electronics and Applications Conference, IEEE*, 2018.

[7] N. Bessous, S. E. Zouzou, W. Bentrah, S. Sbaa, and M. Sahraoui, **"Diagnosis of Bearing Defects In Induction Motors using Discrete Wavelet Transform,"** *International Journal of System Assurance Engineering and Management*, pp. 335-343, 2018.

[8] J. Martinez, A. Belahcen, and A. Muetze, **"Analysis of the Vibration Magnitude of an Induction Motor with Different Numbers of Broken Bars,"** *IEEE transactions on industry applications*, pp. 2711-2720, 2017.

[9] G. H. Bazan, P. R. Scalassara, W. Endo, A. Goedtel, W. F. Godoy, and R. H. C. Palácios, **"Stator Fault Analysis Of Three-Phase Induction Motors Using Information Measures and Artificial Neural Networks,"** *Electric Power Systems Research*, pp. 347-356, 2017.

[10] A. Mejia-Barron, A., M. Valtierra-Rodriguez, D. Granados-Lieberman, J. C. Olivares-Galvan, and R. Escarela-Perez, **"The Application of EMD-based Methods for Diagnosis of Winding Faults in A Transformer Using Transient and Steady State currents,"** *Measurement*, pp. 371-379, 2018.

[11] N. Bessous, S. E. Zouzou, and A. Chemsa, **"A New Analytical Model Dedicated to Diagnose the Rolling Bearing Damage in Induction Motors-Simulation and Experimental Investigation,"** *in Control Engineering and Information Technology Conference (CEIT), IEEE*, pp. 1-9, 2016.

[12] M. Ojaghi, and R. Akhondi, **"Modeling Induction Motors Under Mixed Radial-Axial Asymmetry of the Air Gap Produced By Oil-Whirl Fault in A Sleeve Bearing",** *IEEE Trans. Mag.*, 2018.

[13] C. Kumar, G. Krishnan, and S. Sarangi, **"Experimental Investigation on Misalignment Fault Detection In Induction Motors Using Current and Vibration Signature Analysis",** in *Futuristic Trends on Computational Analysis and Knowledge Management IEEE*, 61-66 2015.

[14] C. Wang, X. Bao, S. Xu, Y. Zhou, W. Xu, , and Y. Chen, **"Analysis of Vibration And Noise For Different Skewed Slot-Type Squirrel-Cage Induction Motors",** *IEEE Trans. Mag.*, pp. 1-6 2017.

[15] K. K. Nallamekala, **"Harmonic Cancellation Technique of Four Pole Induction Motor Drive by Using Phase Shifted Carrier Space Vector PWM Technique,"** *Majlesi Journal of Electrical Engineering*, 12(2), pp. 21-28, 2018.

[16] R. K. Patel, S. Agrawal, and N. C. Joshi, **"Induction Motor Bearing Fault Identification Using Vibration Measurement,"** *in Engineering and Systems (SCES)*, pp. 1-5, 2012.